

Three-point correlation functions in Yang-Mills theory

Marcela Peláez^{ab}, Matthieu Tissier^a, and Nicolás Wschebor^b

^a*LPTMC, Laboratoire de Physique Théorique de la Matière Condensée,
CNRS UMR 7600, Université Pierre et Marie Curie,
boite 121, 4 pl. Jussieu, 75252 Paris Cedex 05, France.*

^b*Instituto de Física, Facultad de Ingeniería, Universidad de la República,
J. H. y Reissig 565, 11000 Montevideo, Uruguay.*

(Dated: June 14, 2021)

We investigate the three-point correlation functions of Yang-Mills theory in the Landau gauge, with a particular emphasis on the infrared regime. The effect of the Gribov copies is accounted for by adding a mass term for the gluons in the Faddeev-Popov action in the Landau gauge. We perform a one-loop calculation for the ghost-antighost-gluon and three-gluon correlation functions. These analytic results are compared with the available lattice data and give a very satisfying agreement.

PACS numbers: Valid PACS appear here

Keywords:

I. INTRODUCTION

The physical observables of gauge theories are associated with gauge-invariant quantities, which are therefore of utmost interest. However in most of the analytical or semi-analytical approaches, the determination of the expectation values of these gauge-invariant quantities rely on understanding also the gauge-dependent sector of the theory. This is one of the reasons why so much effort has been devoted to understand the properties of correlation functions in Yang Mills theories in the past.

Several techniques are used to study these quantities. From the analytic side, standard perturbation theory (that make use of the Faddeev-Popov construction) is the most efficient tool to access the ultraviolet regime of the theory, but fails at momenta of the order of 1 GeV. Indeed, the effective coupling (which is the expansion parameter of perturbation theory) is large in this regime. The standard perturbation theory even predicts that the coupling constant diverges at the so-called infrared (IR) Landau pole. For the low-energy regime, the preferred analytical techniques are nonperturbative renormalization-group and Schwinger-Dyson equation methods [1–15]. These rely on a set of exact equations that are truncated, by making some ansatz on a sector of the theory.

Another technique that has been used is lattice simulations that have played a central role in our understanding of the correlation functions, in particular in the Landau gauge which is rather easy to implement in simulations. The extensive numerical work that has been performed in the past decades [16–20], in conjunction with various semi-analytical techniques including various SD studies, allowed to settle the controversy between two possible solutions of Schwinger-Dyson equations. The so-called scaling solution corresponds to a gluon propagator that tend to zero at low momentum and a ghost dressing function (the propagator multiplied by the momentum squared) that diverges in this limit [1–5, 13]. The so-called massive or decoupling solution gives a finite gluon propagator

and a regular ghost dressing function at low momentum [5, 8–12, 14, 15]. Lattice simulations clearly favored the second option in dimensions higher than two and the first one in the two-dimensional case [17, 21].

In the past years, two of us have developed a new approach to access the infrared behavior of the correlation functions. It relies on the fact that, as is well known since the work of Gribov [22], the Faddeev-Popov construction which is at the heart of most of the analytical approaches, is not fully justified [50]. This is due to the fact that this procedure does not completely fix the gauge. This so-called Gribov ambiguity is however known to be unimportant in the high momentum regime, and is only susceptible of modifying the infrared properties. The idea pushed forward in [26, 27] consists in modeling the influence of the Gribov copies by adding a mass term for the gluons to the usual Faddeev-Popov action (this leads to the Curci-Ferrari model in the Landau gauge [28]). This idea was made more precise in [29] where a new Landau gauge-fixing was proposed, which takes into account the Gribov ambiguity from first principles and which leads, as far as perturbation theory is concerned, to the same results as those obtained with the massive extension considered in [26, 27]. A one-loop calculation for the gluon propagator and the ghost dressing function was performed that compared very well with lattice simulations in $d = 4$, with a maximum error of $\sim 10\%$, both for $SU(2)$ and $SU(3)$.

It may look surprising that the infrared (often called nonperturbative) regime of the theory can be reproduced to that level of precision with a modest one-loop calculation. Our interpretation of this fact is that the mass regularizes the theory in the infrared. For example, we found renormalization schemes where the Landau pole disappears. Moreover we made in [27] an estimate showing that, in the infrared regime, the loop corrections to the propagators are suppressed by powers of the external momenta (in particular, the 2-loop corrections are roughly an order of magnitude smaller than the one-loop contributions), which indicates that the perturbation theory *in*

presence of a mass term may be under control.

These encouraging results naturally lead us to consider other correlation functions. In consequence, in this article, we generalize our previous work to 3-point correlation functions. These functions are extremely interesting for many reasons:

- They have been calculated in lattice simulations [30–36] and this offers concrete data to compare with.
- Once the parameters of the model have been fixed for the 2-point functions, the calculation of 3-point functions becomes a *pure prediction* without any parameter to adjust. This then becomes a very challenging test of the scheme proposed in [26, 27].
- These functions are much richer than 2-point functions. In particular, instead of depending on a single momentum, they depend on three independent momenta squared. Moreover, they include various tensorial structures that could make their study even richer (even if these structures have not yet been studied by lattice simulations).

In the past few years, several works aimed at describing these 3-point correlation functions in the infrared regime, both with lattice simulations [30–36] and with semi-analytical methods [15, 37–39]. However, the complexity of the standard semi-analytical methods (as Schwinger-Dyson equations or Non-Perturbative Renormalization Group equations) have delayed their study. In particular very few results on the ghost-antighost-gluon vertex are available [15, 37–39] and essentially only models for the 3-gluon vertex have been proposed (see, for example, [15]). On the contrary, the scheme developed in [26, 27] and that we follow here relies on a standard and simple 1-loop calculation. Our main aim in this article is to show that we obtain 3-point vertex functions which reproduce very well the lattice data for a relatively small computational effort. Note that Gracey [40] studied the power corrections to the perturbative ultraviolet behaviour both in the model considered here and in the refined Gribov-Zwanziger model. These corrections are different so that lattice simulations with good precision would allow to make a definite difference between both methods.

The outline of the article is the following. In Section II, we describe in more details the model and present our one-loop calculation. We then describe in Section III the renormalization schemes that we implemented and finally describe our results and compare them to the lattice data available for the 3-point correlation functions in Section IV. We give our conclusions in Section V.

II. ONE-LOOP CALCULATION

Our starting point is the Curci-Ferrari action in the Landau gauge, written in Euclidean space, that reads:

$$S = \int d^d x \left[\frac{1}{4} F_{\mu\nu}^a F_{\mu\nu}^a + i h^a \partial_\mu A_\mu^a + \partial_\mu \bar{c}^a (D_\mu c)^a + \frac{1}{2} m_0^2 (A_\mu^a)^2 \right] \quad (1)$$

where the covariant derivative applied to a field X in the adjoint representation reads $(D_\mu X)^a = \partial_\mu X^a + g_0 f^{abc} A_\mu^b X^c$, g_0 is the bare coupling constant, f^{abc} are the structure constants of the gauge group and $F_{\mu\nu}^a = \partial_\mu A_\nu^a - \partial_\nu A_\mu^a + g_0 f^{abc} A_\mu^b A_\nu^c$ is the field strength. Apart for the bare mass m_0 of the gluons, the action is that of the Yang-Mills theory with the Faddeev-Popov action in the Landau gauge. All our analytical calculations will be done for a generic $SU(N)$ gauge group.

The Feynman rules are the standard ones, except for the free propagator of the gluon which reads:

$$\langle A_\mu^a A_\nu^b \rangle_0(p) = \delta^{ab} P_{\mu\nu}^\perp(p) \frac{1}{p^2 + m_0^2} \quad (2)$$

where we introduced the transverse projector (and, for later use, the longitudinal one):

$$P_{\mu\nu}^\perp(p) = \delta_{\mu\nu} - \frac{p_\mu p_\nu}{p^2} \quad (3)$$

$$P_{\mu\nu}^\parallel(p) = \frac{p_\mu p_\nu}{p^2} \quad (4)$$

Instead of computing the correlation functions, we compute as usual the vertex functions which are obtained by considering only the one-particle irreducible (1PI) diagrams. We parametrize the two-point vertex functions in terms of three scalar functions:

$$\Gamma_{A_\mu^a A_\nu^b}^{(2)}(p) = \delta^{ab} (\Gamma^\perp(p) P_{\mu\nu}^\perp + \Gamma^\parallel(p) P_{\mu\nu}^\parallel) \quad (5)$$

$$\Gamma_{c^a \bar{c}^b}^{(2)}(p) = \delta^{ab} \frac{p^2}{J(p)} \quad (6)$$

The full propagators for the gluon and ghost then read:

$$\langle A_\mu^a A_\nu^b \rangle(p) = \delta^{ab} \frac{P_{\mu\nu}^\perp(p)}{\Gamma^\perp(p)} \quad (7)$$

$$\langle c^a \bar{c}^b \rangle(p) = \delta^{ab} \frac{J(p)}{p^2} \quad (8)$$

The function J is the so-called dressing functions. The 1-loop expressions for Γ^\perp and J were computed in [26, 27]. The longitudinal part of the gluon two-point function is not directly accessible in lattice simulations and was therefore not considered in the past. It proved however interesting to compute it because it appears in some Ward identities that we used to check the consistency of our results. The 1-loop expressions for these three functions are given in the supplemental material [41].



FIG. 1: One-loop Feynman diagrams for the ghost-antighost-gluon vertex.

A. Ghost-antighost-gluon vertex

The one-loop calculation for the ghost-antighost-gluon vertex function requires computing the two Feynman diagrams showed in Fig. 1. The tensorial structure is rather simple. At one loop, the vertex is proportional to f^{abc} where a , b and c are respectively the color indices of the ghost, antighost and gluon external legs. We will consider here and below only this color structure. This is an exact property for $SU(2)$, and for general $SU(N)$, it remains true at two loops and also in the large N limit. However, this is only an approximation for $SU(3)$ (currently used in the literature [42]). The Lorentz index μ of the gluon external leg can be carried by one of the external momenta. Because of the momentum conservation, there are actually only two scalar components. Following Ball and Chiu [42], it is however convenient to express the vertex in terms of a rank two tensor $\Gamma_{\nu\mu}$ such that:

$$\Gamma_{c^a \bar{c}^b A_\mu^c}^{(3)}(p, k, r) = -ig_0 f^{abc} k_\nu \Gamma_{\nu\mu}(p, k, r) \quad (9)$$

with

$$\begin{aligned} \Gamma_{\nu\mu}(p, k, r) = & \delta_{\mu\nu} a(r^2, k^2, p^2) \\ & - r_\nu p_\mu b(r^2, k^2, p^2) + k_\nu r_\mu c(r^2, k^2, p^2) \\ & + r_\nu k_\mu d(r^2, k^2, p^2) + k_\nu k_\mu e(r^2, k^2, p^2) \end{aligned} \quad (10)$$

Note that lattice simulations access the vertex function only through the correlation function, *i.e.* the vertex function with external legs contracted with the full propagators. Since the gluon propagator is transverse, the function c is not accessible to lattice simulations. In fact, the lattice simulations on the ghost-antighost-gluon correlation function that have actually been performed [36] are presented in terms of a scalar function which is obtained by contracting the external gluon leg with the transverse propagator and with the bare ghost-antighost-gluon vertex, normalized by the same expression at tree level:

$$G^{c\bar{c}A}(p, k, r) = \frac{k_\nu P_{\mu\nu}^\perp(r) k_\rho \Gamma_{\rho\mu}(p, k, r)}{k_\nu P_{\mu\nu}^\perp(r) k_\mu} \quad (11)$$

A simple calculation shows that this correlation function depends on a unique linear combination of the scalar functions defined in (10):

$$a + k \cdot r (b + d) + k^2 e \quad (12)$$

with the functions a, b, d and e evaluated at (r^2, k^2, p^2) . Although this is the only available numerical data, it is interesting to compute the 5 scalar functions a, b, c, d and e because this gives an internal check of the validity of the calculation, see below. Moreover, future lattice studies may lead to a determination of the various tensorial components independently.

In our calculations, we decomposed each diagram on the tensorial structure of Eq. (10), following the ideas of [43]. We can then deduce the contribution of a diagram to each of the scalar functions a to e in terms of integrals. To do so, it is convenient to rewrite the product of a massive propagator and of a massless propagator as:

$$\frac{1}{p^2(p^2 + m^2)} = \frac{1}{m^2} \left(\frac{1}{p^2} - \frac{1}{p^2 + m^2} \right) \quad (13)$$

We can thus express the scalar functions in terms of a few simple integrals. By using Feynman parameters, we can perform the momentum integral and obtain expressions with at most one integral over a Feynman parameter that cannot be performed analytically for generic momentum configurations. The expression are lengthy and not particularly instructive. We give them in the supplemental material [41]. The calculation simplifies in the case of one vanishing external momentum. In particular, when the ghost or antighost momentum vanishes, the vertex function have no loop corrections [44]. For vanishing gluon momentum, the vertex is non-trivial and we find, in $d = 4 - \epsilon$:

$$\begin{aligned} \Gamma_{\mu\nu}(p, -p, 0) = & \delta_{\mu\nu} \left\{ 1 + \frac{g_0^2 N}{128\pi^2} \left[9/2 + s \right. \right. \\ & + 5s^{-1} - (7s^{-1} + 5s^{-2}) \log(s + 1) \\ & \left. \left. - (s - 1)s \log(s^{-1} + 1) \right] \right\} \end{aligned} \quad (14)$$

where we introduced $s = p^2/m^2$. Note that the previous (bare) vertex is finite due to the non-renormalization theorem to be discussed below. The equivalent expression in $d = 3$ reads:

$$\begin{aligned} \Gamma_{\mu\nu}(p, -p, 0) = & \delta_{\mu\nu} \left\{ 1 + \frac{g_0^2 N}{384\pi m s} \left[2(6s^2 \right. \right. \\ & - 5s - 21) - 3\pi\sqrt{s}(2s^2 - s + 288) \\ & \left. \left. + 6s^{-1/2}(2s^3 - s^2 - 68s + 7) \arctan(\sqrt{s}) \right] \right\} \end{aligned} \quad (15)$$

B. Three gluon vertex

The one-loop calculation for the three-gluon correlation function requires computing the three Feynman diagrams showed in Fig. 2. Again, the color structure is rather simple at one loop, being proportional to f^{abc} . As for the ghost-antighost-gluon vertex, we will ignore the

possibility of more involved color structures (that are absent at two-loops order, for $SU(2)$ gauge group and also in the large N limit of $SU(N)$ gauge groups) Accordingly, we define:

$$\Gamma_{A_\mu^a A_\nu^b A_\rho^c}^{(3)}(p, k, r) = -ig_0 f^{abc} \Gamma_{\mu\nu\rho}(p, k, r).$$

The Lorentz structure is richer than in the previous case since there are now three Lorentz indices. We have used the decomposition of Ball and Chiu [42] to extract six scalar functions:

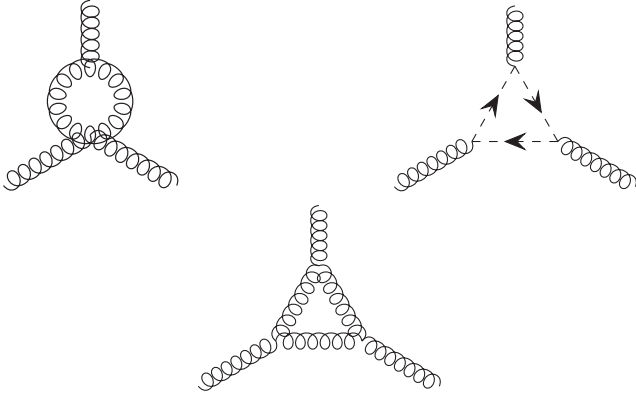


FIG. 2: One-loop Feynman diagrams for the 3-gluon vertex.

$$\begin{aligned} \Gamma_{\mu\nu\rho}(p, k, r) = & A(p^2, k^2, r^2) \delta_{\mu\nu} (p - k)_\rho + B(p^2, k^2, r^2) \delta_{\mu\nu} (p + k)_\rho - C(p^2, k^2, r^2) (\delta_{\mu\nu} p \cdot k - p_\nu k_\mu) (p - k)_\rho \\ & + \frac{1}{3} S(p^2, k^2, r^2) (p_\rho k_\mu r_\nu + p_\nu k_\rho r_\mu) + F(p^2, k^2, r^2) (\delta_{\mu\nu} p \cdot k - p_\nu k_\mu) (p_\rho k \cdot r - k_\rho p \cdot r) \\ & + H(p^2, k^2, r^2) \left[-\delta_{\mu\nu} (p_\rho k \cdot r - k_\rho p \cdot r) + \frac{1}{3} (p_\rho k_\mu r_\nu - p_\nu k_\rho r_\mu) \right] + \text{cyclic permutations} \end{aligned} \quad (16)$$

The scalar functions have the following symmetry properties: A , C and F are symmetric under permutation of the first two arguments; B is antisymmetric under permutation of the first two arguments; H is completely symmetric and S is completely antisymmetric. As for the ghost-antighost-gluon vertex, only a subset of these functions are measurable in lattice simulations; when the external legs are contracted with the gluon propagators (which is transverse), the functions B and S disappear. In lattice simulations [36], the quantity which has been considered is a scalar function obtained by contracting the external legs of the vertex with transverse propagators and the tree-level momentum structure of the 3-gluon vertex, normalized to the same expression at the bare level:

$$G^{AAA}(p, k, r) = \frac{[(r - k)_\gamma \delta_{\alpha\beta} + \text{cyclic permutations}] P_{\alpha\mu}^\perp(p) P_{\beta\nu}^\perp(k) P_{\gamma\rho}^\perp(r) \Gamma_{\mu\nu\rho}(p, k, r)}{[(r - k)_\gamma \delta_{\alpha\beta} + \text{cyclic permutations}] P_{\alpha\mu}^\perp(p) P_{\beta\nu}^\perp(k) P_{\gamma\rho}^\perp(r) [(r - k)_\rho \delta_{\mu\nu} + \text{cyclic permutations}]} \quad (17)$$

The scalar functions A , B , C , S , F and H are computed in the same way as described above. Our expression for generic momenta involve at most one integral over a Feynman parameter and cannot be expressed in terms of elementary functions. They are given in the supplemental material [41]. When one momentum vanishes, the integral

over the Feynman parameter can be performed analytically which simplifies considerably the results. For $d = 4 - \epsilon$:

$$\begin{aligned}
\Gamma_{\mu\nu\rho}(p, 0, -p) = & \left\{ 1 - \frac{Ng_0^2}{768\pi^2} \left[-\frac{136}{\epsilon}(1 - \epsilon \log \bar{m}) + \frac{1}{3}(36s^{-2} - 594s^{-1} + 319 + 6s) + (3s^2 - 2) \log s \right. \right. \\
& - 4s^{-3}(1+s)^3(s^2 - 9s + 3) \log(1+s) \\
& \left. \left. + \frac{(4+s)^{3/2}}{s^{3/2}} (24 - 30s + s^2) \log \left(\frac{\sqrt{4+s} + \sqrt{s}}{\sqrt{4+s} - \sqrt{s}} \right) \right] \right\} (p_\mu \delta_{\nu\rho} + p_\rho \delta_{\mu\nu}) \\
& - \left\{ 2 + \frac{Ng_0^2}{384\pi^2} \left[-\frac{136}{\epsilon}(1 - \epsilon \log \bar{m}) + \frac{1}{3}(18s^{-2} - 321s^{-1} - 97 + 24s) + (s-1)(s^2 - 2s - 2) \log s \right. \right. \\
& - 2s^{-3}(1+s)^2(s-1)(s^3 - 7s^2 + 7s - 3) \log(1+s) \\
& \left. \left. + \frac{\sqrt{4+s}}{s^{3/2}} (48 + 16s + 22s^2 - 11s^3 + s^4) \log \left(\frac{\sqrt{4+s} + \sqrt{s}}{\sqrt{4+s} - \sqrt{s}} \right) \right] \right\} p_\nu \delta_{\mu\rho} \\
& - \frac{Ng_0^2}{384\pi^2 m^2} \left[(-36s^{-3} + 278s^{-2} - 74s^{-1} - 10) - s^2 \log s \right. \\
& \left. + s^{-3}(1+s)^2(36s^{-1} - 44 - 4s - 12s^2 + 2s^3) \log(1+s) \right. \\
& \left. + \sqrt{s(4+s)} s^{-3} (-144s^{-1} + 80 + 4s + 10s^2 - s^3) \log \left(\frac{\sqrt{4+s} + \sqrt{s}}{\sqrt{4+s} - \sqrt{s}} \right) \right] p_\mu p_\nu p_\rho
\end{aligned} \tag{18}$$

where $\bar{m}^2 = m^2 e^\gamma / (4\pi)$ with γ the Euler constant. The divergent term $\propto 1/\epsilon$ disappears once the renormalized vertex functions are expressed in terms of the renormalized parameters, see Sect. III.

In $d = 3$, the same quantity reads:

$$\begin{aligned}
\Gamma_{\mu\nu\rho}(p, 0, -p) = & \left\{ 1 - \frac{Ng_0^2}{128\pi m \sqrt{s}} \left[\frac{\pi}{2}(2 - 3s^2) + \frac{2}{3s^{3/2}}(3s^3 + 23s^2 + 56s - 15) \right. \right. \\
& \left. \left. - s^{-1}(4+s)(16 - 18s + s^2) \arctan(\sqrt{s}/2) + 2s^{-2}(s-5)(s+1)^2 \arctan(\sqrt{s}) \right] \right\} (p_\mu \delta_{\nu\rho} + p_\rho \delta_{\mu\nu}) \\
& - \left\{ 2 + \frac{Ng_0^2}{128\pi m \sqrt{s}} \left[\pi(-s^3 + 3s^2 - 1) + \frac{2}{3s^{3/2}}(15s^3 - 51s^2 + 53s - 15) \right. \right. \\
& \left. \left. + 2(-s^3 + 6s^2 + 2s - 16 - 32s^{-1}) \arctan(\sqrt{s}/2) + 2(2s^3 - 9s^2 - 5)(1 - s^{-2}) \arctan(\sqrt{s}) \right] \right\} p_\nu \delta_{\mu\rho} \\
& - \frac{Ng_0^2}{128\pi m^3 \sqrt{s}} \left[\pi(s^{-1} + s^2) + \frac{2}{3s^{5/2}}(-21s^3 + 5s^2 - 139s + 75) \right. \\
& \left. + 2s^{-2}(s^4 - 5s^3 - 16s^2 - 40s + 96) \arctan(\sqrt{s}/2) \right. \\
& \left. - 2s^{-3}(s+1)(2s^4 - 7s^3 - 9s^2 - 15s + 25) \arctan(\sqrt{s}) \right] p_\mu p_\nu p_\rho
\end{aligned} \tag{19}$$

C. Checks

We present in this section the different checks that can be performed on our one-loop expressions. First, as explained in the Appendix, the vertex functions fulfill the following Slavnov-Taylor identity:

$$\begin{aligned}
& [\Gamma^\perp(p)P_{\mu\rho}^\perp(p) + \Gamma^\parallel(p)P_{\mu\rho}^\parallel(p)]\Gamma_{\mu\nu}(r, p, k) \\
& - [\Gamma^\perp(k)P_{\mu\nu}^\perp(k) + \Gamma^\parallel(k)P_{\mu\nu}^\parallel(k)]\Gamma_{\mu\rho}(r, k, p) \\
& = r_\mu J^{-1}(r)\Gamma_{\rho\nu\mu}(p, k, r)
\end{aligned} \tag{20}$$

We have verified analytically that our one-loop expressions satisfy this relation. This gives a nontrivial check for most of the scalar functions, except however F and H which are associated with transverse momentum structures and that do not appear in Eq. (20).

Second, we have compared our expressions in the limit of vanishing mass with those of [45]. Because we used the relation (13), there appear in our expressions terms in $1/m$ that would naively diverge in the limit of small mass. We can check explicitly that the limit is actually regular but the analytic comparison is cumbersome. We have made instead a numerical comparison of our expres-

sions and those of [45] for 50 momentum configurations, taking the mass of the gluon much smaller than the momenta. We have mainly considered the scalar functions appearing in the ghost-antighost-gluon vertex (10) and the functions F and H that, as discussed above, are not constrained by Eq. (20). In all cases, our expressions in the massless limit agree with [45] at the numerical precision level.

Finally we have considered the following equality, which is derived in the Appendix.

$$\begin{aligned} \tilde{\Gamma}_\mu(p, k, r) + \tilde{\Gamma}_\mu(k, p, r) - \frac{r_\mu}{r^2} \left[\frac{p_\nu}{p^2} \tilde{\Gamma}_\nu(k, r, p) \right. \\ \left. + \frac{k_\nu}{k^2} \tilde{\Gamma}_\nu(p, r, k) \right] = 0 \end{aligned} \quad (21)$$

where

$$\tilde{\Gamma}_\mu(p, k, r) = k_\nu \Gamma_{\nu\mu}(p, k, r) r^2 J^{-1}(r) \quad (22)$$

To our knowledge this relation have not been derived before. We have checked numerically for 50 momentum configurations that the previous identity is indeed satisfied, with no constraint on the mass.

D. Infrared behavior

It is instructive to discuss the behavior of the different vertex functions when all the external momenta are much smaller than the mass scale. A straightforward analysis shows that, in this limit, the leading contribution comes from the diagram with as much ghost propagators as possible. Multiplying all momenta by a common coefficient κ , we obtain the following behaviors, valid in arbitrary dimension:

$$\begin{aligned} \Gamma_{\mu\nu}(\{\kappa p_i\}) - \delta_{\mu\nu} \sim \kappa^{d-2}, \\ \Gamma_{\mu\nu\rho}(\{\kappa p_i\}) \sim \kappa^{d-4}. \end{aligned} \quad (23)$$

As a consequence of these behavior, G^{AAA} diverges as $\log \kappa$ in $d = 4$ and diverges as $1/\kappa$ in $d = 3$ when $\kappa \rightarrow 0$.

III. RENORMALIZATION AND RENORMALIZATION GROUP

In this section, we describe the renormalization schemes that we implemented and explain how the renormalization-group ideas are implemented. As we explain below, some care must be taken when comparing the (bare) lattice data with the renormalized analytical results.

A. Renormalization and schemes

As usual, the divergences appearing in the one-loop expressions can be absorbed into a redefinition of the

coupling constant, mass and fields. In $d = 3$ no ultra-violet divergences are present but a (finite) renormalization is done anyway in order to be able to exploit renormalization-group methods and improve perturbation theory. We define the renormalized quantities as:

$$\begin{aligned} A_0^{a\mu} = \sqrt{Z_A} A^{a\mu}, \quad c_0^a = \sqrt{Z_c} c^a, \quad \bar{c}_0^a = \sqrt{Z_{\bar{c}}} \bar{c}^a, \\ g_0 = Z_g g \quad m_0^2 = Z_{m^2} m^2 \end{aligned} \quad (24)$$

From now on, except when explicitly stated, all quantities are the renormalized ones. The relations between bare (with subindices ‘‘0’’) and renormalized vertices are the following:

$$\begin{aligned} \Gamma_{A_\mu^a A_\nu^b}^{(2)}(p) &= Z_A \Gamma_{A_\mu^a A_\nu^b, 0}^{(2)}(p) \\ \Gamma_{c^a \bar{c}^b}^{(2)}(p) &= Z_c \Gamma_{c^a \bar{c}^b, 0}^{(2)}(p) \\ \Gamma_{c^a \bar{c}^b A_\mu^c}^{(3)}(p, r) &= Z_c \sqrt{Z_A} \Gamma_{c^a \bar{c}^b A_\mu^c, 0}^{(3)}(p, r) \\ \Gamma_{A_\mu^a A_\nu^b A_\rho^c}^{(3)}(p, r) &= Z_A^{3/2} \Gamma_{A_\mu^a A_\nu^b A_\rho^c, 0}^{(3)}(p, r) \end{aligned} \quad (25)$$

We have used two renormalization schemes to fix the renormalization factors, that were already presented in [27]. The vanishing-momentum (VM) scheme is characterized by

$$\begin{aligned} \Gamma^\perp(p = \mu) &= m^2 + \mu^2, \quad J(p = \mu) = 1 \\ \Gamma^\perp(p = 0) &= m^2. \end{aligned} \quad (26)$$

The infrared safe scheme (IS) relies on a non-renormalization theorem for the mass [46–48] (this non-renormalization theorem was conjectured in [49]), which is imposed here for the finite part of the renormalization parameters. It is defined by:

$$\begin{aligned} \Gamma^\perp(p = \mu) &= m^2 + \mu^2, \quad J(p = \mu) = 1, \\ Z_{m^2} Z_A Z_c &= 1. \end{aligned} \quad (27)$$

In both cases, we use the Taylor scheme to fix the renormalization factor of the coupling constant. This leads to:

$$Z_g \sqrt{Z_A} Z_c = 1 \quad (28)$$

The explicit expressions for the different renormalization factors are given in [27].

It is important to relate the objects observed on lattice simulations $G_0^{c\bar{c}A}$ and G_0^{AAA} given by Eqs. (11) and (17) to the renormalized vertices. The quantities that are used on the lattice are bare vertices without renormalization factors. When expressed in terms of the renormalized vertices as in Eq. (25), we obtain:

$$\begin{aligned} G_0^{c\bar{c}A}(p, k, r) &= G^{c\bar{c}A}(p, k, r) \\ G_0^{AAA}(p, k, r) &= \frac{Z_c}{Z_A} G^{AAA}(p, k, r) \end{aligned} \quad (29)$$

where the renormalized expressions correspond to those written in Eqs. (11) and (17) but with the corresponding renormalized vertices instead of the bare ones. In

order to arrive to this result we exploited the Taylor's non-renormalization theorem (28). Of course, the lattice results are regularized and accordingly the factor Z_c/Z_A is finite but it is necessary to include it when comparing our renormalized results to those coming from lattice simulations.

B. Renormalization Group

Once the correlation functions for the renormalized field are expressed in terms of the renormalized coupling constant and renormalized mass, we get finite expressions both in $d = 3$ and in $d = 4$. The direct comparison of these expressions with the lattice results was not completely satisfactory at energies of a few GeV. This is to be attributed to large loop corrections (in $d = 4$ large logarithms $\propto \log(p/\mu)$) and we therefore had to use a renormalization-group improvement of our one-loop expressions. To do so, we introduce the β function and anomalous dimensions of the fields as:

$$\beta_g(g, m^2) = \mu \left. \frac{dg}{d\mu} \right|_{g_0, m_0^2}, \quad (30)$$

$$\beta_{m^2}(g, m^2) = \mu \left. \frac{dm^2}{d\mu} \right|_{g_0, m_0^2}, \quad (31)$$

$$\gamma_A(g, m^2) = \mu \left. \frac{d \log Z_A}{d\mu} \right|_{g_0, m_0^2}, \quad (32)$$

$$\gamma_c(g, m^2) = \mu \left. \frac{d \log Z_c}{d\mu} \right|_{g_0, m_0^2}. \quad (33)$$

We can then use the RG equation for the vertex function with n_A gluon legs and n_c ghost legs:

$$\left(\mu \partial_\mu - \frac{1}{2} (n_A \gamma_A + n_c \gamma_c) + \beta_g \partial_g + \beta_{m^2} \partial_{m^2} \right) \Gamma^{(n_A, n_c)} = 0, \quad (34)$$

to relate these functions at different scales:

$$\Gamma^{(n_A, n_c)}(\{p_i\}, \mu, g(\mu), m^2(\mu)) = z_A(\mu)^{n_A/2} z_c(\mu)^{n_c/2} \times \Gamma^{(n_A, n_c)}(\{p_i\}, \mu_0, g(\mu_0), m^2(\mu_0)). \quad (35)$$

where $g(\mu)$ and $m^2(\mu)$ are obtained by integration of the beta functions with initial conditions given at some scale μ_0 and:

$$\begin{aligned} \log z_A(\mu) &= \int_{\mu_0}^{\mu} \frac{d\mu'}{\mu'} \gamma_A(g(\mu'), m^2(\mu')), \\ \log z_c(\mu) &= \int_{\mu_0}^{\mu} \frac{d\mu'}{\mu'} \gamma_c(g(\mu'), m^2(\mu')). \end{aligned} \quad (36)$$

There remains to choose the RG scale μ at which Eq. (35) is evaluated. For a correlation function with typical momentum p , in the UV regime $p \gg m$, it is important to take $\mu \simeq p$. However, in the IR regime, the

theory is effectively massive and no large logarithm are present. It is therefore not necessary to integrate the flow down to RG scales smaller than m . We therefore used a running scale: [51]

$$\mu = \sqrt{p^2 + \alpha m^2(\mu_0)} \quad (37)$$

where α is a parameter that, in principle, can vary between zero and values of order one. In practice we used various values of α between 0 and 3. We discuss for the two schemes and for $d = 4$ and $d = 3$ the dependence on α in the following section.

IV. RESULTS

In this section, we present the results for the 2 and 3-point functions both in $d = 4$ and in $d = 3$. As explained in [26, 27] the perturbative scheme considered here does not work in $d = 2$. In that case, the loop corrections contains infrared divergences that a IR Landau-pole remains present, even if a mass for the gluons have been introduced. For this reason, we only present results for higher dimensions.

A. Fixing parameters

Following [26, 27], we consider here the values of the mass and coupling constants at some renormalization scale μ_0 as fitting parameters. Since the lattice results are much more precise for the propagators than for the 3-point correlation functions, we look for the set of parameters that lead to the best fit of the 2-point correlation functions. [Note that the global normalization of the ghost and gluon two-point correlation functions are not accessible so we have to introduce a multiplicative factor in front of our analytic expression of the propagators, which must be fixed by comparison with the lattice data.] The values of the mass and coupling constant thus determined are then used for computing the 3-point correlation function. When comparing the latter with lattice results, we are thus left with only one free parameter associated with the global normalization of G^{AAA} . For each lattice parameter beta, we fixed this multiplicative factor by considering a particular momentum configuration (with one vanishing momentum) and used the same value for the other momentum configurations [52]. In previous work we compared both the $SU(2)$ and the $SU(3)$ cases with lattice results [26, 27]. In the present article, given that the available lattice simulations for the infrared behaviour of 3-point functions are for the $SU(2)$ group, we only present numerical results for that case.

When comparing lattice data with analytical results, it is important to have simultaneously a small relative and absolute error since the propagators tend to zero in the ultraviolet. Therefore, we use the following indicators to

quantify the precision of our results:

$$\begin{aligned}\chi_{AA}^2 &= \frac{1}{4N} \sum_i (\Gamma_{\text{lt.}}^\perp(\mu_0)^2 + \Gamma_{\text{lt.}}^\perp(p_i)^2) \left(\frac{1}{\Gamma_{\text{lt.}}^\perp(p_i)} - \frac{1}{\Gamma_{\text{th.}}^\perp(p_i)} \right)^2 \\ \chi_{c\bar{c}}^2 &= \frac{1}{4N} \sum_i (J_{\text{lt.}}^{-2}(\mu_0) + J_{\text{lt.}}^{-2}(p_i)) (J_{\text{lt.}}(p_i) - J_{\text{th.}}(p_i))^2\end{aligned}\quad (38)$$

It corresponds to a sort of average between the (normalized) absolute error and the relative error. In order to chose the parameters we took a value that gives a compromise between optimal values for both propagators. We analyzed the errors for various values of α in both schemes both in $d = 4$ and in $d = 3$. For moderate values of α (between 1 and 3) we do not observe an important dependence on α . In the VM scheme, if the parameter α is too small, the system shows a IR Landau pole and the results do not fit well the lattice data. For that scheme we chose $\alpha = 1$ and all results presented in that scheme corresponds to that value. In the IS scheme, there is no Landau pole. For the $d = 4$ case, the curves are almost insensitive to α , even when it tends to 0. In the $d = 3$ case, the best fits are obtained for $\alpha = 0$. In the following, all our results in the IS scheme are given for $\alpha = 0$. The corresponding values are presented in Tables I and II.

As our 1-loop expressions are certainly not exact and given a certain tolerance of the estimate of the propagators, there are many possible values of the associated parameters. In Fig. 3 we present the contour levels associated to errors 4, 7 and 10% for the quantities χ_{AA} and $\chi_{c\bar{c}}$ both in $d = 4$ and $d = 3$ in schemes IS and VM. We can see that there is a region of acceptable parameters (with errors in both 2-point functions lower than 10%) in almost all cases. The only exception is the VM scheme in $d = 3$. In that dimension, the IS scheme is much more precise than the other (and in fact gives an excellent fit for both 2-point functions simultaneously). The same observation is also true for the 3-point functions discussed below. We observe that there is a large degeneracy of possible acceptable values for the parameters compatible with lattice data for the ghost propagator. On the contrary, fitting the gluon propagator is much more demanding and the region of acceptable parameters is much smaller.

Scheme	α	g_0	m_0 (GeV)
IS	0.0	5.2	0.44
IS	1.0	5.2	0.43
IS	2.0	5.8	0.48
IS	3.0	6.3	0.53
VM	1.0	7.5	0.77
VM	2.0	9.0	0.78
VM	3.0	9.1	0.75

TABLE I: Fitting parameters retained for computing correlation functions in $d = 4$ for different schemes.

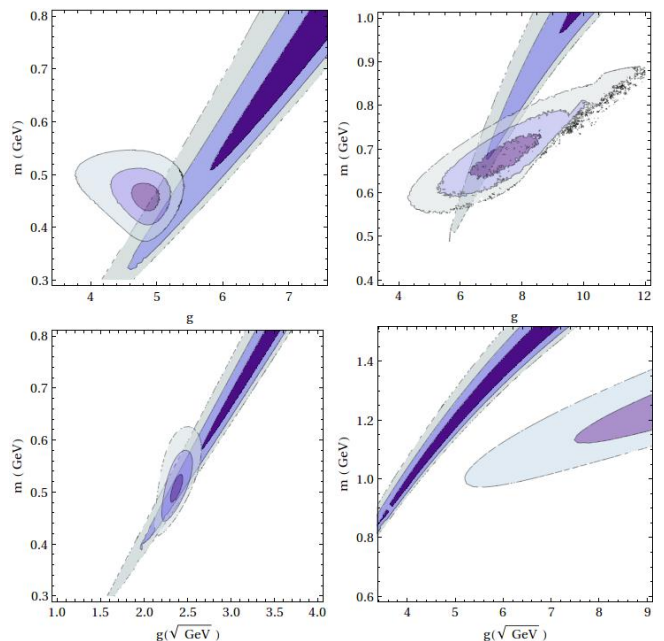


FIG. 3: Contour levels for the quantities χ_{AA} and $\chi_{c\bar{c}}$ for the IS scheme (left) and VM scheme (right), both for $d = 4$ (above) and $d = 3$ (below). The large diagonal region corresponds to chi cc and the small elliptic one to chi AA. From dark to light: 4%, 7% and 10%.

B. $d = 4$

We first present the results for the gluon propagator and the ghost dressing function. The β functions were integrated with initial condition at $\mu_0 = 1$ GeV and we used the values of the mass and coupling constants given in Table I.

For all these schemes, we find a good agreement with the lattice data, with an error in-between 5 and 10% for χ_{AA} and $\chi_{c\bar{c}}$. However, the ghost-antighost-gluon vertex functions are best reproduced with the VM scheme. We also present curves with the IS scheme. The difference between the two sets of curves gives an indication of the error of our calculation.

The gluon propagator and ghost dressing functions are depicted in Fig. 4. We show in Fig. 5 our results for $G^{c\bar{c}A}$ and in Fig. 6 for G^{AAA} for different momentum configurations.

In all cases, the results are compared with the corresponding results obtained in lattice simulations [36]. The agreement is excellent. It is a striking result that the set of parameters adapted for describing the 2-point correlation function gives simultaneously a good agreement for the 3-point functions. When comparing the results with lattice data, it is important to note that the data for the 3-point functions (particularly for the G^{AAA} functions) have large statistical errors and a full analysis of systematic errors has not been done yet. In consequence we can not completely neglect the errors coming from the lattice data with respect to those coming from the present

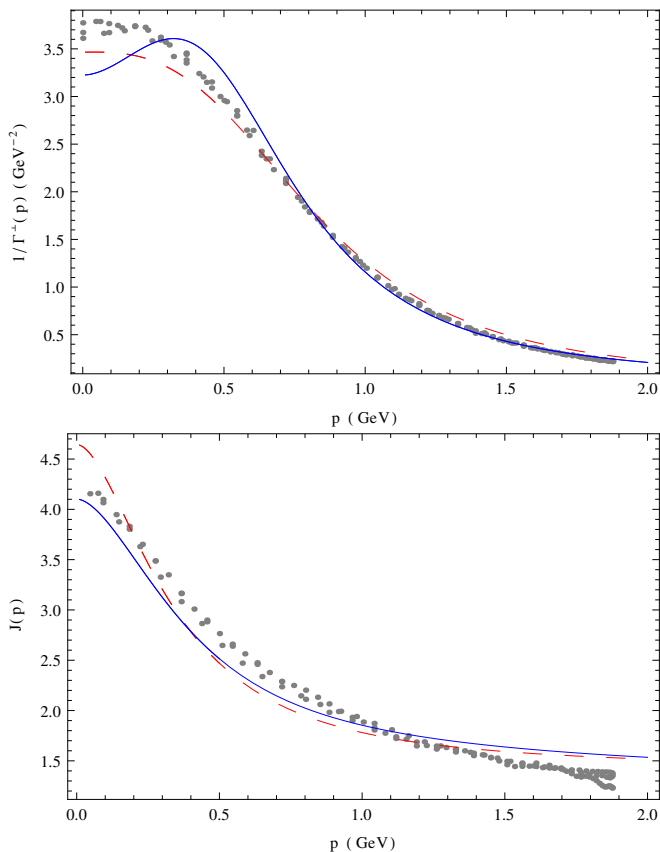


FIG. 4: Gluon propagator (top) and ghost dressing function (bottom) as a function of momentum in $d = 4$. The points are lattice data of [16]. The plain line (color online blue) corresponds to the infrared safe scheme with $\alpha = 0$; the dashed line (color online red) corresponds to the vanishing momentum scheme with $\alpha = 1$.

calculation.

C. $d = 3$

A similar analysis can be performed in $d = 3$. We summarize in Table II the parameters retained for the different renormalization schemes. As explained before,

Scheme	α	g_0 ($\text{GeV}^{1/2}$)	m_0 (GeV)
IS	0.0	2.4	0.55
IS	1.0	2.5	0.55
IS	2.0	2.5	0.55
IS	3.0	3.0	0.65
VM	1.0	4.0	1.00
VM	2.0	4.5	0.95
VM	3.0	6.1	1.11

TABLE II: Fitting parameters retained for computing correlation functions in $d = 3$ for different schemes.

the VM scheme does not give results with good simultaneous agreement with lattice data for both propaga-

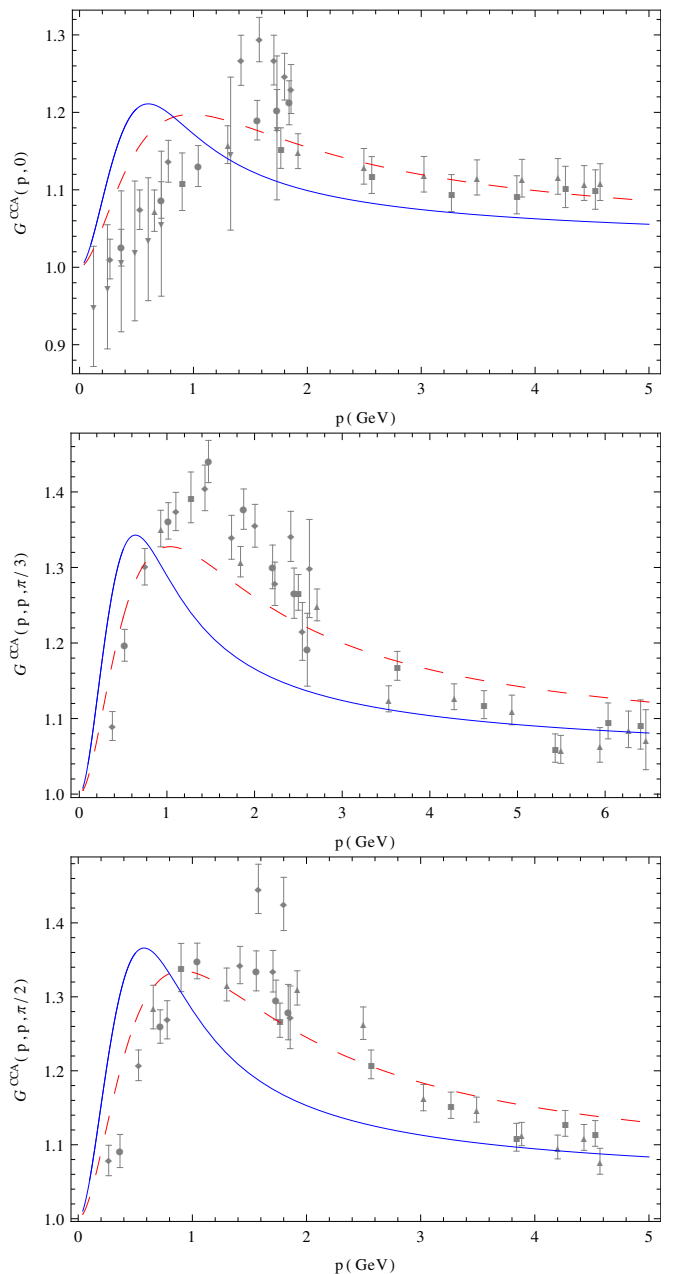


FIG. 5: Ghost-antighost-gluon correlation function $G^{c\bar{c}A}$ for one vanishing momentum (top figure), all momenta equal (middle figure), two momenta orthogonal, of equal norm (bottom) as a function of momentum, in $d = 4$. The lattice data of [36] are compared with our calculations. See caption of Fig. 4 for the legend.

tors. However, there is an excellent agreement in the IS scheme (with errors in-between 5 and 10% for χ_{AA} and $\chi_{\bar{c}c}$). In particular the IS scheme correctly reproduces the increase of the gluon propagator at low momentum. The best choice for α is zero. We do not have a solid argument explaining why the preferred renormalization scheme is different in $d = 4$ and in $d = 3$. The gluon propagator and ghost dressing functions are depicted in Fig. 7. The

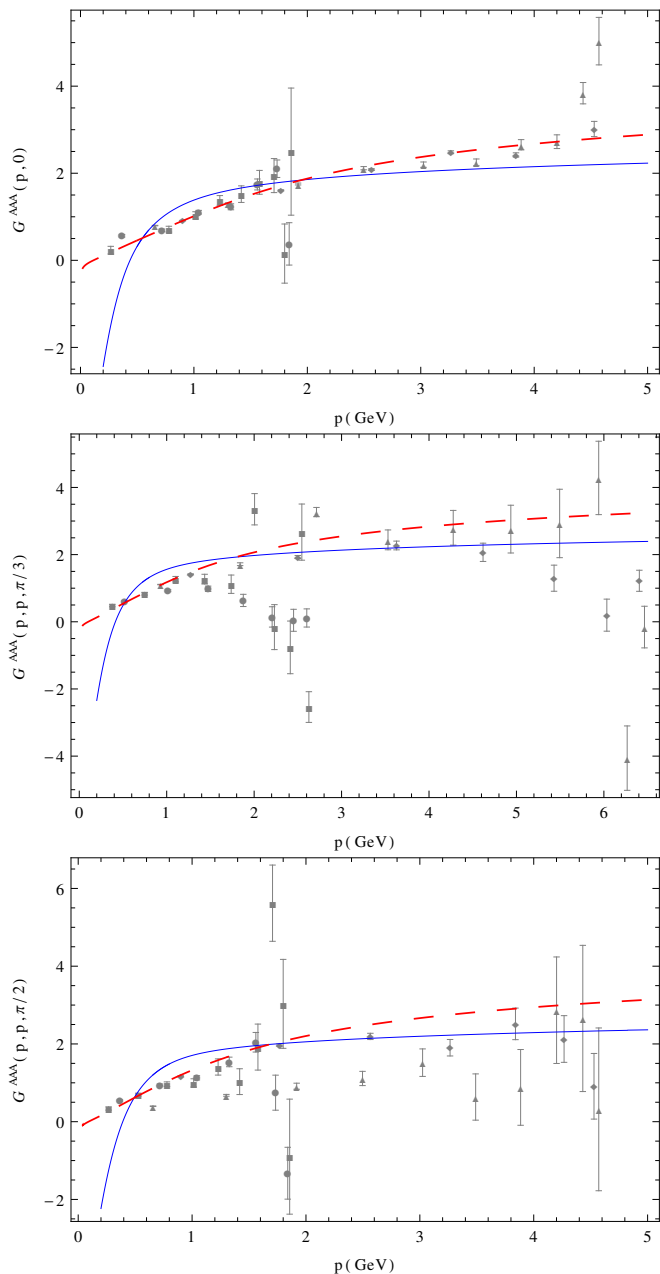


FIG. 6: Three gluon correlation function G^{AAA} for one vanishing momentum (top figure), all momenta equal (middle figure), two momenta orthogonal, of equal norm (bottom) as a function of momentum, in $d = 4$. The lattice data of [36] are compared with our calculations. See caption of Fig. 4 for the legend.

agreement remains very good and, moreover, all qualitative aspects of the curves are correctly reproduced. In particular, we find that the G^{AAA} becomes negative at small momenta and diverges for vanishing momenta, in agreement with lattice results [53].

We show in Fig. 8 our results for $G^{c\bar{c}A}$ and in Fig. 9 for G^{AAA} for different momentum configurations. As for the four dimensional case, we used the parameters that

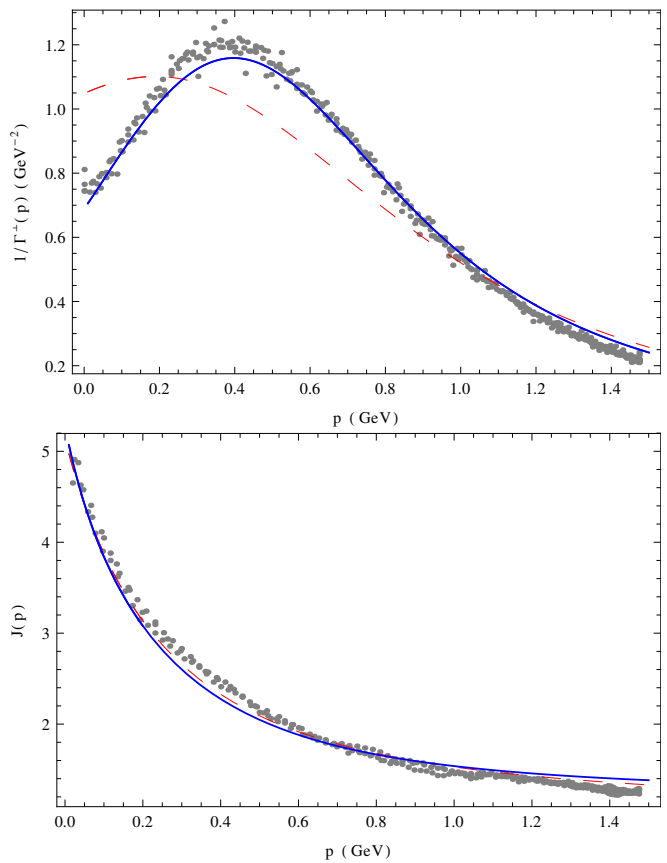


FIG. 7: Gluon propagator (top) and ghost dressing function (bottom) as a function of momentum in $d = 3$. The points are lattice data of [16]. The plain line (color online blue) corresponds to the infrared safe scheme with $\alpha = 0$; the dashed line (color online red) corresponds to the vanishing momentum scheme with $\alpha = 1$.

lead to the best fits for the 2-point functions as inputs in our calculation of the 3-point functions. Consequently those functions are calculated without any free parameter (with the exception of the renormalization factor for the G^{AAA} function mentioned previously). We obtain a very good agreement as in $d = 4$.

V. CONCLUSIONS

In the present article we have presented a perturbative calculation of 3-point correlation functions in Landau-gauge, Yang-Mills theories in $d = 4$ and $d = 3$ in all momentum regimes including the infrared. Very few analytical results were known up to now for infrared behavior of the ghost-antighost-gluon vertex [15, 37–39]. For the 3-gluon functions only educated ansatzes have been proposed previously (see [15] and references therein). Following [26, 27], we introduced a bare gluon mass so as to obtain controlled perturbative expressions both in the ultraviolet and in the infrared regime and gives an infrared-safe perturbative expansion for non-exceptional momen-

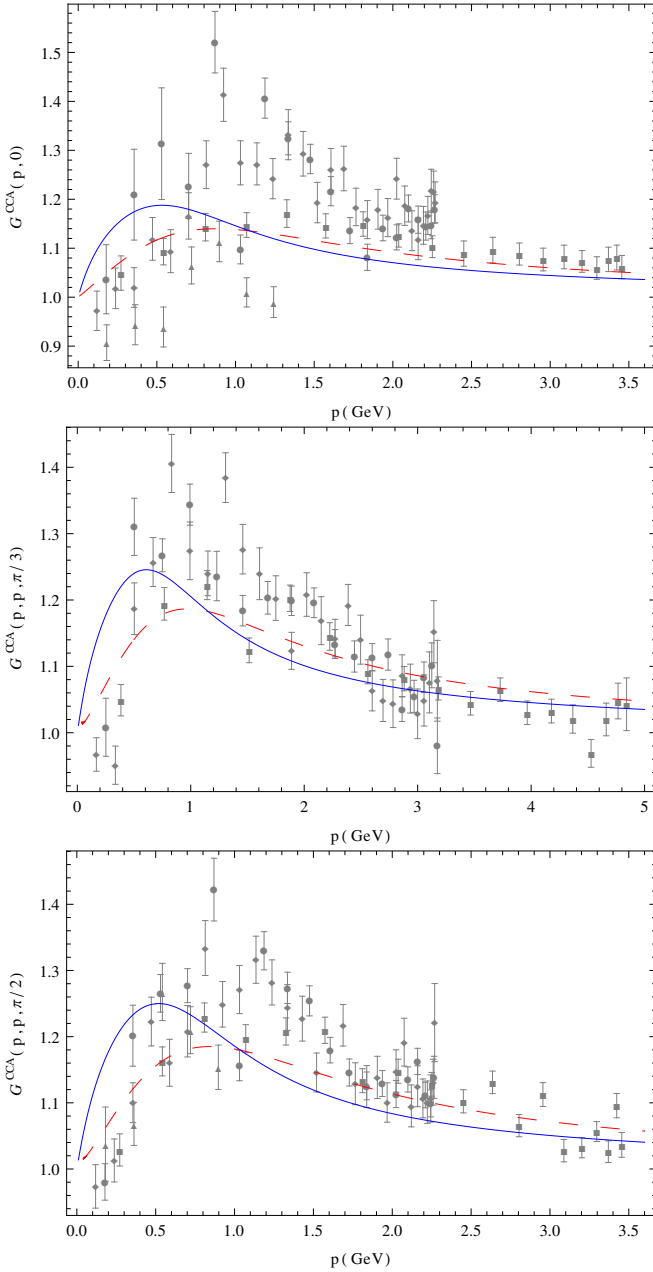


FIG. 8: Ghost-antighost-gluon correlation function $G^{c\bar{c}A}$ for one vanishing momentum (top figure), all momenta equal (middle figure), two momenta orthogonal, of equal norm (bottom) as a function of momentum, in $d = 3$. The lattice data of [36] are compared with our calculations. See caption of Fig. 7 for the legend.

tum configurations for all $d > 2$. Note that, in the gauge-fixing procedure of [29], the mass-term naturally appears in the process of lifting of the Gribov ambiguity.

We fixed the parameters of the model by fitting the 2-point function to lattice simulations and by using two families of renormalization group schemes. The resulting parameters are then used to calculate the 3-point functions. The comparison of the resulting functions with lat-

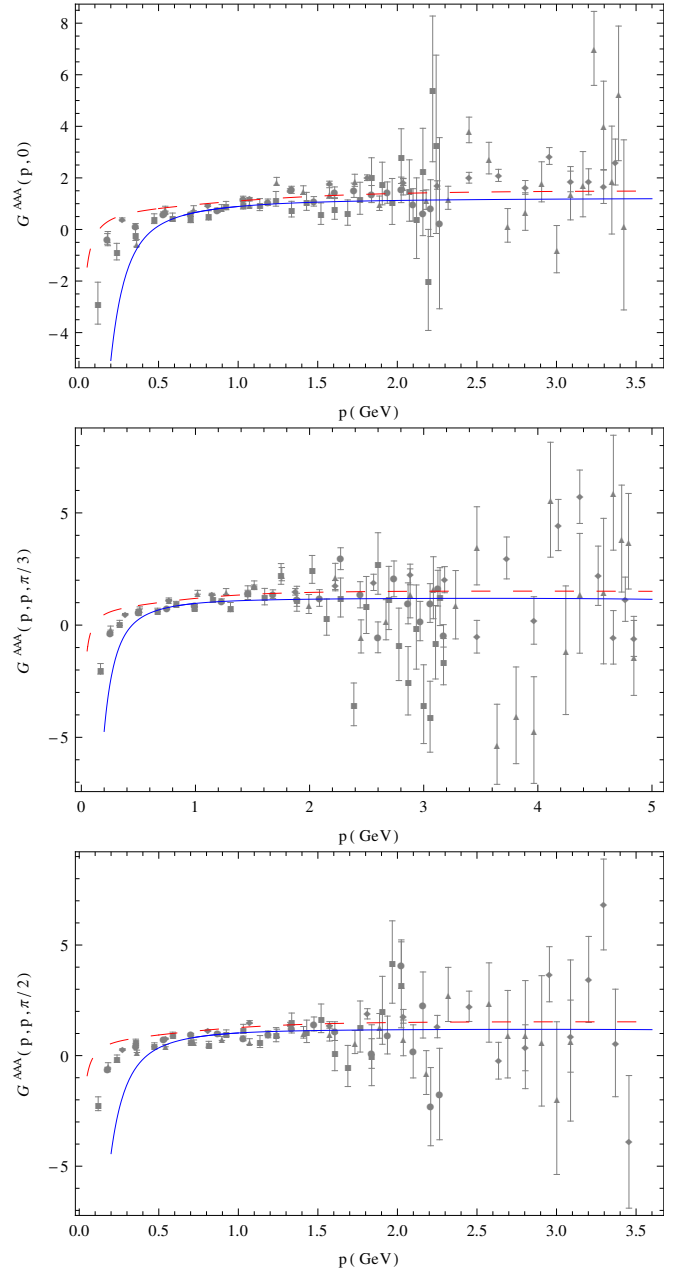


FIG. 9: Three gluon correlation function G^{AAA} for one vanishing momentum (top figure), all momenta equal (middle figure), two momenta orthogonal, of equal norm (bottom) as a function of momentum, in $d = 3$. The lattice data of [36] are compared with our calculations. See caption of Fig. 7 for the legend.

tice simulations is therefore performed without any extra free-parameter (with the only exception of a renormalization factor in the G^{AAA} function) and is very good. First, all qualitative properties observed in lattice correlators are correctly explained in a simple way. For example, it is observed in lattice simulations that the 3-gluon correlator becomes negative in $d = 3$ at low momenta and even seems to diverge when all momenta go to zero. This

is a consequence of the IR divergence of the diagrams with ghost loops when all momenta go to zero. Second, not only the qualitative agreement is very good, but also the comparison with lattice simulations gives an excellent quantitative agreement. Note that the available lattice data still have large statistical errors and more precise results (possibly with other tensor structures) would be welcome to give sharper test of our findings.

All these results strongly support the idea that at least an important part of the infrared effects present in Quantum Chromodynamics can take its origin in the Gribov-copies as has been suggested in last years [22–25]. Contrarily to previous analysis of these effects, the present approach does not require the introduction of extra fields and the Feynman rules remain almost identical to those of the standard perturbative analysis. Only the gluon mass parameter is new and the calculation of many correlators become treatable in practice, as shown in the present article. Consequently, these studies can be extended in many aspects. We are currently considering also the introduction of quarks that can be done very easily. We also started studying the influence of higher loop contributions to the 2-point correlation functions.

Of course, there are many open questions to be analyzed in the future. First of all, the inclusion of a mass term violates the nilpotency of standard BRST transformations. Even if this difficulty is present in all approaches that take into account in various ways Gribov-copies effects, it has major consequences. In particular, standard definition of the physical space of non-abelian gauge theories, based in the cohomology of the BRST charge is no longer applicable. A new definition of the physical space is then required in order to be able to control the unitarity of the S matrix on it. This is a major problem that clearly goes beyond the present article and that we would like to consider in the future.

Acknowledgments

The authors want to acknowledge A. Maas for kindly making available the lattice data and for useful exchanges. They want also acknowledge M. Q. Huber and J. A. Gracey for useful suggestions. The authors want acknowledge partial support from PEDECIBA and ECOS programs. N. W. wants to thanks the LPTMC (UPMC), where most of the present work has been done, for its hospitality.

Appendix A: BRST symmetry

In this appendix, we derive several constraints on the vertex functions that can be deduced from the symmetries of the theory. We recall that the action is invariant under the Becchi-Rouet-Stora-Tiutin (BRST) transfor-

mation:

$$\begin{aligned}\delta A_\mu^a &= \zeta(\partial_\mu c^a + g_0 f^{abc} A_\mu^b c^c), \\ \delta c^a &= \zeta(-\frac{1}{2}g_0 c^b c^c), \\ \delta \bar{c}^a &= \zeta i h^a, \quad \delta i h^a = \zeta m_0 c^a.\end{aligned}\tag{A1}$$

where ζ is a Grassmann parameter. As usual, we introduce sources for the BRST variations of the fields A and c with the following action:

$$\begin{aligned}S_{\text{sources}} &= \int_x \left[\bar{K}_\mu^a (\partial_\mu c^a + g_0 f^{abc} A_\mu^b c^c) \right. \\ &\quad \left. - \frac{g_0}{2} f^{abc} \bar{L}^a c^b c^c \right].\end{aligned}\tag{A2}$$

The Slavnov-Taylor (ST) identity associated with this symmetry reads:

$$\begin{aligned}\int d^d x \left\{ \frac{\delta \Gamma}{\delta A_\mu^a} \frac{\delta \Gamma}{\delta \bar{K}_\mu^a} + \frac{\delta \Gamma}{\delta c^a} \frac{\delta \Gamma}{\delta \bar{L}^a} - i h^a \frac{\delta \Gamma}{\delta \bar{c}^a} \right. \\ \left. + i m_0^2 \frac{\delta \Gamma}{\delta h^a} c^a \right\} = 0\end{aligned}\tag{A3}$$

We will also make use of the symmetry:

$$\begin{aligned}\delta A_\mu^a = \delta c^a = 0, \quad \delta \bar{c}^a = \epsilon c^a, \\ \delta i h^a = -\epsilon \frac{g_0}{2} f^{abc} c^b c^c.\end{aligned}\tag{A4}$$

where ϵ is an infinitesimal real number. The associated ST identity reads:

$$\int d^d x \left\{ c^a \frac{\delta \Gamma}{\delta \bar{c}^a} + i \frac{\delta \Gamma}{\delta h^a} \frac{\delta \Gamma}{\delta \bar{L}^a} \right\} = 0\tag{A5}$$

Finally, we can write a Ward identity associated with the invariance of the theory under an infinitesimal shift in the antighost $\bar{c}(x) \rightarrow \bar{c}(x) + \epsilon(x)$, which reads:

$$\partial_\mu \frac{\delta \Gamma}{\delta \bar{K}_\mu^a(x)} = \frac{\delta \Gamma}{\delta \bar{c}^a(x)}\tag{A6}$$

Deriving this equation once with respect to c and taking the Fourier transform, we find:

$$-i p_\mu \Gamma_{c^b \bar{K}_\mu^a}^{(2)}(p) = \Gamma_{c^b \bar{c}^a}^{(2)}(p)\tag{A7}$$

Deriving once more with respect to A and taking the Fourier transform, we obtain:

$$-i p_\mu \Gamma_{c^a \bar{K}_\mu^b A_\nu^c}^{(3)}(p, k, r) = \Gamma_{c^a \bar{c}^b A_\nu^c}^{(3)}(p, k, r)\tag{A8}$$

This last expression justifies the tensorial decomposition (9) and shows that:

$$\Gamma_{c^a \bar{K}_\nu^b A_\mu^c}^{(3)}(p, k, r) = -i g f^{abc} \Gamma_{\nu\mu}(p, k, r)\tag{A9}$$

if we suppose a color structure proportional to f^{abc} , as was done all along this article.

We can now prove Eq. (20) by deriving Eq. (A3) with respect to \bar{c} and twice with respect to A and expressing the vertex involving \bar{K} by using Eqs. (A7,A8).

Eq. (21) is obtained much in the same way. we first derive Eq. (A3) with respect to two ghost and one antighost fields, and Fourier transform. We thus get:

$$\begin{aligned} & -\Gamma_{c^c\bar{c}^b A_\mu^d}^{(3)}(k, r, p)\Gamma_{c^a\bar{K}_\mu^d}^{(2)}(p) + \Gamma_{c^a\bar{c}^b A_\mu^d}^{(3)}(p, r; k)\Gamma_{c^c\bar{K}_\mu^d}^{(2)}(k) \\ & + \Gamma_{c^d\bar{c}^b}^{(2)}(r)\Gamma_{c^a c^c\bar{L}^d}^{(3)}(p, k; r) = 0 \end{aligned} \quad (\text{A10})$$

The vertex that involves \bar{L} can be re-expressed by deriving Eq. (A5) with respect to A and to c twice, and Fourier transforming:

$$\Gamma_{c^d\bar{c}^c A_\mu^b}^{(3)}(p, k; r) - \Gamma_{c^c\bar{c}^d A_\mu^b}^{(3)}(k, p; r) + ir_\mu\Gamma_{c^d c^c\bar{L}^b}^{(3)}(p, k; r) = 0 \quad (\text{A11})$$

The last two equations can be used to prove (21) using again, a color structure proportional to f^{abc} .

-
- [1] L. von Smekal, R. Alkofer and A. Hauck, Phys. Rev. Lett. **79** (1997) 3591.
- [2] R. Alkofer and L. von Smekal, Phys.Rept.**353** (2001) 281.
- [3] D. Zwanziger, Phys. Rev. D **65** (2002) 094039.
- [4] C. S. Fischer and R. Alkofer, Phys. Rev. D **67** (2003) 094020.
- [5] J. C. R. Bloch, Few Body Syst. **33** (2003) 111.
- [6] J. M. Pawłowski, D. F. Litim, S. Nedelko and L. von Smekal, Phys. Rev. Lett. **93**, 152002 (2004) [hep-th/0312324].
- [7] C. S. Fischer and H. Gies, JHEP **0410**, 048 (2004) [hep-ph/0408089].
- [8] A. C. Aguilar and A. A. Natale, JHEP **0408** (2004) 057.
- [9] Ph. Boucaud *et al.*, JHEP **06** (2006) 001.
- [10] A. C. Aguilar and J. Papavassiliou, Eur. Phys. J. A **35** (2008) 189.
- [11] A. C. Aguilar, D. Binosi and J. Papavassiliou, Phys. Rev. D **78** (2008) 025010.
- [12] P. Boucaud, J. P. Leroy, A. Le Yaouanc, J. Micheli, O. Pene and J. Rodriguez-Quintero, JHEP **06** (2008) 099.
- [13] C. S. Fischer, A. Maas and J. M. Pawłowski, Annals Phys. **324** (2009) 2408.
- [14] J. Rodriguez-Quintero, JHEP **1101** (2011) 105.
- [15] M. Q. Huber and L. von Smekal, JHEP **04**, 149 (2013) arXiv:1211.6092 [hep-th].
- [16] A. Cucchieri and T. Mendes, Phys. Rev. Lett. **100** (2008) 241601 and also arXiv:1001.2584 [hep-lat].
- [17] A. Cucchieri and T. Mendes, Phys. Rev. D **78** (2008) 094503.
- [18] A. Cucchieri and T. Mendes, Phys. Rev. D **81** (2010) 016005.
- [19] I. L. Bogolubsky *et al.*, Phys. Lett. B **676**, 69 (2009).
- [20] D. Dudal, O. Oliveira and N. Vandersickel, Phys. Rev. D **81** (2010) 074505.
- [21] A. Maas, Phys. Rev. D **75** (2007) 116004.
- [22] V. N. Gribov, Nucl. Phys. B **139** (1978) 1.
- [23] D. Zwanziger, Nucl. Phys. B **323**, 513 (1989).
- [24] D. Zwanziger, Nucl. Phys. B **399**, 477 (1993).
- [25] D. Dudal, J. A. Gracey, S. P. Sorella, N. Vandersickel and H. Verschelde, Phys. Rev. D **78** (2008) 065047.
- [26] M. Tissier and N. Wschebor, Phys. Rev. D **82** (2010) 101701 [arXiv:1004.1607 [hep-ph]].
- [27] M. Tissier and N. Wschebor, Phys. Rev. D **84** (2011) 045018 [arXiv:1105.2475 [hep-th]].
- [28] G. Curci and R. Ferrari, Nuovo Cim. A **32**, 151 (1976).
- [29] J. Serreau and M. Tissier, Phys. Lett. B **712** (2012) 97 [arXiv:1202.3432 [hep-th]].
- [30] C. Parrinello, Phys. Rev. D **50** (1994) 4247 [hep-lat/9405024].
- [31] B. Alles, D. Henty, H. Panagopoulos, C. Parrinello, C. Pittori and D. G. Richards, Nucl. Phys. B **502** (1997) 325 [hep-lat/9605033].
- [32] P. Boucaud, J. P. Leroy, J. Micheli, O. Pene and C. Roiesnel, JHEP **9810** (1998) 017 [hep-ph/9810322].
- [33] A. Cucchieri, T. Mendes and A. Mihara, JHEP **0412** (2004) 012 [hep-lat/0408034].
- [34] E.-M. Ilgenfritz, M. Muller-Preussker, A. Sternbeck and A. Schiller, hep-lat/0601027.
- [35] A. Cucchieri, A. Maas and T. Mendes, Phys. Rev. D **74** (2006) 014503 [hep-lat/0605011].
- [36] A. Cucchieri, A. Maas and T. Mendes, Phys. Rev. D **77**, 094510 (2008) [arXiv:0803.1798 [hep-lat]].
- [37] J. Rodriguez-Quintero, PoS QCD -TNT-II, 040 (2011) [arXiv:1112.4749 [hep-ph]].
- [38] D. Dudal, O. Oliveira and J. Rodriguez-Quintero, Phys. Rev. D **86** (2012) 105005 [arXiv:1207.5118 [hep-ph]].
- [39] A. C. Aguilar, D. Ibáñez and J. Papavassiliou, Phys. Rev. D **87**, 114020 (2013) [arXiv:1303.3609 [hep-ph]].
- [40] J. A. Gracey, Phys. Rev. D **86**, 105029 (2012) [arXiv:1210.5962 [hep-th]].
- [41] Mathematica file with all our results for the scalar functions appearing in the two and three-point correlation functions.
- [42] J. S. Ball and T.-W. Chiu, Phys. Rev. D **22** (1980) 2550–2557
- [43] G. Passarino and M. J. G. Veltman, Model, Nucl. Phys. B **160** (1979) 151.
- [44] J. C. Taylor, Nucl. Phys. B **33** (1971) 436.
- [45] A. I. Davydychev and P. Osland and O. V. Tarasov, Phys. Rev. D **54** (1996) 4087–4113
- [46] D. Dudal, H. Verschelde and S. P. Sorella, Phys. Lett. B **555** (2003) 126.
- [47] N. Wschebor, Int. J. Mod. Phys. A **23** (2008) 2961.
- [48] M. Tissier and N. Wschebor, Phys. Rev. D **79**, 065008 (2009).
- [49] J. A. Gracey, Phys. Lett. B **552**, 101 (2003) [hep-th/0211144].
- [50] Another approach to study the impact of Gribov copies in the infrared sector of Yang-Mills theory has been followed for many years, mainly by Zwanziger [3, 23–25]. Different approximations performed in that scheme gave propagators compatible with both massive and scaling scenarios.
- [51] A conceptually more satisfying criterion would be to use the mass at the running scale μ instead of μ_0 . However, the variation of the mass is small in the range of energy of interest for us so that the difference between these two schemes is tiny.

[52] In principle, this normalization of G^{AAA} could be fixed by normalizing the lattice results with the gluon and ghost propagators in such a way that the continuum limit is well defined. We would then have one less parameter to fix when comparing with lattice data. This would give a more stringent test of theoretical results.

[53] G^{AAA} also becomes negative in $d = 4$ but at scales much smaller, probably difficult to observe in the lattice. More precisely, we obtain a divergence as $1/p$ in $d = 3$ but only as $\log(p)$ in $d = 4$.